Steady and Unsteady Transonic Flow

H. L. Seegmiller,* J. G. Marvin,† and L. L. Levy Jr.‡
NASA Ames Research Center, Moffett Field, Calif.

The flow over an 18% thick circular arc airfoil at 0-deg angle of attack is studied at two Mach numbers, 0.76 and 0.79, and a single Reynolds number, based on chord, of 11×10^6. At the higher Mach number, shock-induced separation occurred at the foot of the shock wave and extended downstream beyond the trailing edge. At the lower Mach number, shock-induced separation also occurrred, but the flow was unsteady and periodic. The mean velocity, turbulent Reynolds stresses, and kinetic energy were measured with a two-component laser velocimeter. Time-resolved velocity measurements for the unsteady flow were conditionally sampled and the mean velocity field for one cycle of oscillation was determined. During the initial portion of the cycle a shock wave forms near the trailing edge, strengthens, and moves toward the airfoil leading edge. The flow downstream of the shock wave separates and appears to reattach downstream on the airfoil near the trailing edge. A similar sequence takes place on the other side of the airfoil, 180 deg out of phase. Results from a computer code that solves the Reynolds averaged form of the compressible Navier-Stokes equations and employs a mixing length model for the eddy viscosity are compared with the data, and deficiencies are noted.

Nomenclature

a_∞ = speed of sound in the freestream, 305 m/s
ao, bo = alphanumeric symbols for a set of constants from Ref. 21
C_p = pressure coefficient
C_p^* = pressure coefficient evaluated at the local speed of sound
c = airfoil chord
c_f = skin-friction coefficient, $\tau_w / \frac{1}{2}\rho_\infty u_\infty^2$
f = frequency of unsteady flow oscillation
k = turbulent kinetic energy, $\frac{1}{2}(\langle u'^2 \rangle + \langle v'^2 \rangle + \langle w'^2 \rangle)$
L = length scale from Glushko turbulence model
ℓ = Prandtl mixing length
M = Mach number
p = surface pressure
Δp = incremental pressure from the mean surface pressure
Re_c = Reynolds number based on freestream conditions and airfoil chord
t = time measured from the beginning of the oscillating pressure pulse
T = fractional time of one cycle of flow oscillation
u = mean velocity in x direction
V = total mean velocity
v = mean velocity in y direction
$\langle u'^2 \rangle$ = time average of the square of the velocity fluctuation in x direction
$\langle v'^2 \rangle$ = time average of the square of the velocity fluctuation in y direction
$\langle w'^2 \rangle$ = time average of the square of the velocity fluctuation in the spanwise direction
$\overline{u'v'}$ = time averaged velocity correlation
x = distance from the airfoil leading edge in a direction along the horizontal plane of symmetry
y = distance from the airfoil centerline in a direction normal to the horizontal plane of symmetry
$\bar{y}$ = distance from the airfoil surface in a direction normal to the horizontal plane of symmetry
α = angle of attack
$\tilde{\alpha}$ = proportionality constant in Glushko turbulence model
δ = thickness of the shear layer
ϵ = eddy diffusivity, m^2/s
$\bar{\theta}$ = angle of total mean velocity vector relative to the x direction
μ = molecular viscosity
ρ = mean density
τ_t = Reynolds shear stress

Subscripts

DS = dividing streamline
m = mean value
t = total value
∞ = freestream
w = wall value
δ = edge of viscous layer

Presented as Paper 78-160 at the AIAA 16th Aerospace Sciences Meeting, Huntsville, Ala., Jan. 16-18, 1978; submitted Feb. 15, 1978; revision received July 20, 1978. This paper is declared a work of the U.S. Government and therefore is in the public domain.

Index categories: Jets, Wakes and Viscid-Inviscid Flow Interactions; Nonsteady Aerodynamics; Transonic Flow.

*Research Scientist.

†Branch Chief, Experimental Fluid Dynamics Branch. Associate Member AIAA.

‡Research Scientist. Member AIAA.

Introduction

BEFORE this decade, reliable predictive methods for transonic flows depended extensively on experimental data because the complexity of the governing equations made practical solutions impossible. However, the development of large-capacity, fast computers is beginning to change this picture. When viscous effects are small, solutions of the nonlinear inviscid equations are feasible and the results are quite reliable.[1-3] When viscous effects are important and regions of separated flow are large, solutions to the governing equations are also possible, but the results are not reliable enough for predictive purposes primarily because of the lack of an adequate turbulence model.[4]

Experiment and computation are being uniquely coupled to develop turbulence models that can improve the reliability of computational techniques for situations where viscous effects are important.[5,6] One test flow being studied for this purpose is the transonic flow over a thick circular arc airfoil. Several studies of this flow have been reported.[4,7,8] Notable conclusions from these studies are that existing turbulence models are inadequate for quantitative predictions of flows with large separation and that the features of unsteady flow observed experimentally are also observed computationally. Heretofore all of the evidence used to substantiate these conclusions was based on comparisons with measurements taken on the

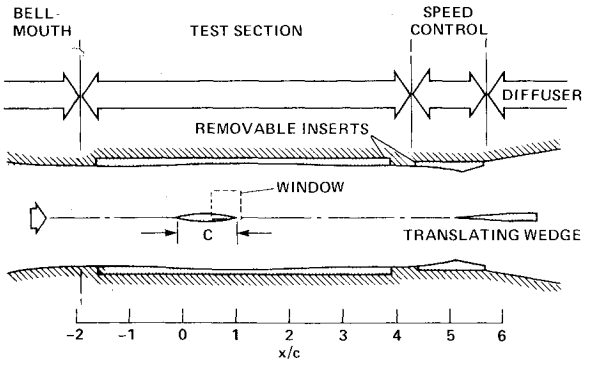

Fig. 1 Experimental arrangement.

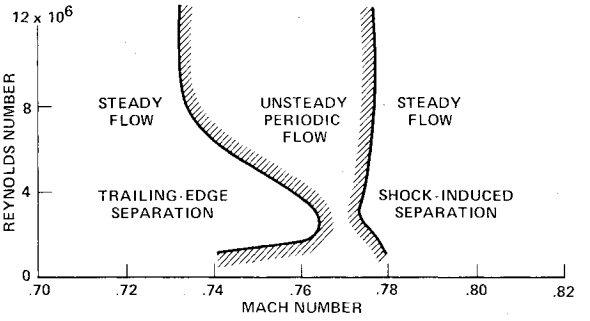

Fig. 2 Experimental flow domains.

surface of the airfoil, so little insight into improving turbulence modeling has been gained and a complete picture of the unsteady flow has been unavailable.

In this paper flowfield data from around the airfoil are presented for both steady and unsteady flows with shock-induced separation. Obtained with a laser velocimeter, the data consist of mean velocity, shear stress, and turbulent kinetic energy profiles in the flowfield downstream of the airfoil midchord where the more complicating features of the flow are present. Computations from a computer code that solves the Reynolds averaged form of the Navier-Stokes equations for both flow situations are compared with these measurements.

Experimental Arrangement and Test Conditions

The test model, a circular arc airfoil with a thickness to chord ratio of 0.18, was tested in the Ames High Reynolds Number Channel at a Reynolds number based on chord of 11×10^6. The experimental arrangement is shown in Fig. 1. The airfoil with a chord of 20.32 cm spanned the shorter dimension of a rectangular test section with dimensions of 38.1 cm by 25.4 cm. The upper and lower walls were contoured to match the inviscid streamlines at $M_\infty = 0.775$ so that the supersonic region of the airfoil flow would not extend to the contoured walls and choke the tunnel.[7] Wall interference effects are thereby reduced but not eliminated. It is important to note, however, that the actual channel wall contours are included in the calculations. Glass windows 14 cm × 14 cm were installed in the side walls of the test section for the purpose of providing optical access for the high-speed shadowgraph movies and the laser velocimeter tests. A translating wedge used in combination with choking inserts established the desired Mach number. The facility operated in a blowdown mode for run times in excess of a minute.

Results from a previous study[7] illustrate the three distinct flow regimes established at the test Mach and Reynolds numbers (Fig. 2). At the test Reynolds number of 11×10^6 and at the lower Mach numbers the flow was steady and trailing-edge separation occurred on the airfoil. For Mach numbers between 0.74 and 0.78 the flow was unsteady but periodic, with shock-induced separation alternating from one side of the airfoil to the other. Above Mach number 0.78 the flow was steady and separation occurred on both sides of the airfoil extending downstream from the foot of the shock wave to beyond the trailing edge. The present test results were obtained at two Mach numbers, 0.76 and 0.79, and the respective flows developed were periodic and steady with shock-induced separation.

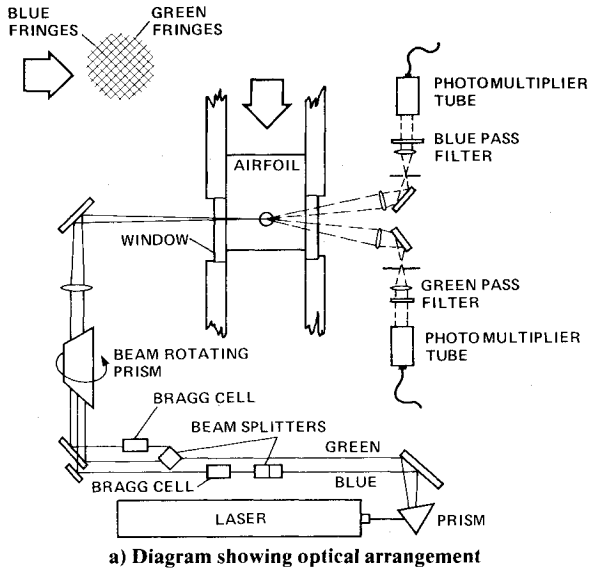

a) Diagram showing optical arrangement

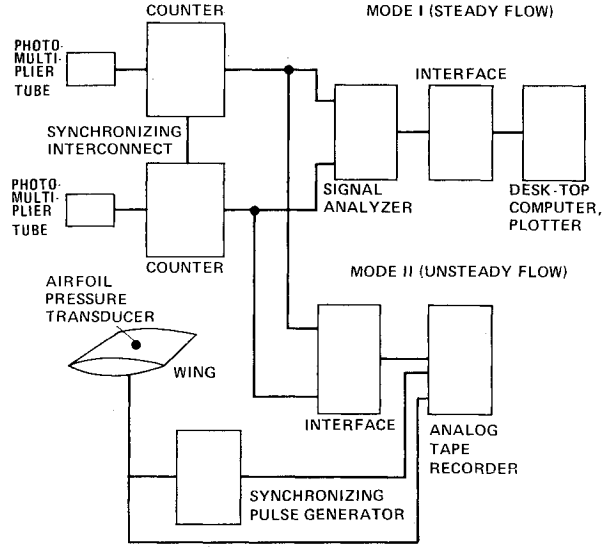

b) Diagram showing data acquisition alternatives

Fig. 3 Laser velocimeter system.

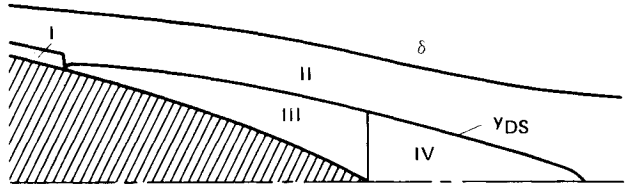

Fig. 4 Boundary-layer and wake regions for turbulence model.

Flowfield Measurements

Mean and fluctuating velocity measurements were made with a two-color laser velocimeter. A schematic of the optical arrangement is shown in Fig. 3a. The two-component system employed a 4-W argon laser using a dispersing prism to obtain beams of 488- and 514.5-nm wavelength. The two

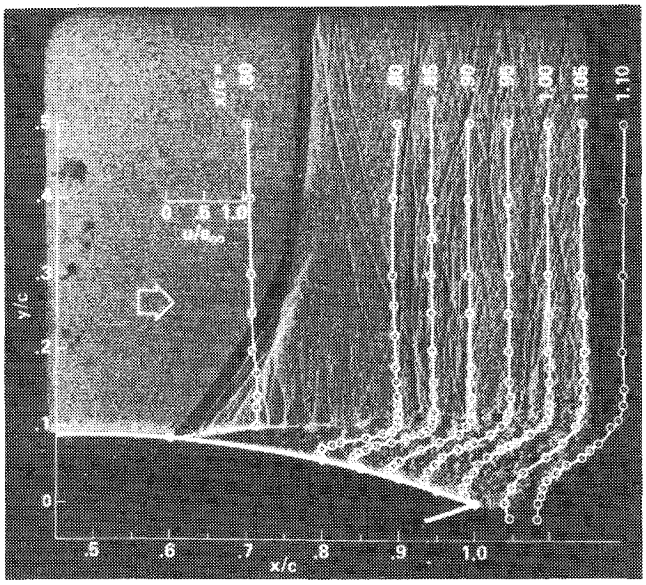

Fig. 5 Shadowgraph of steady shock-induced separation with an overlay showing mean velocity profiles, $M_\infty = 0.79$ and $Re_c = 11 \times 10^6$.

beams were split, rotated ±45 deg, and intersected in the flowfield at a location near the midspan of the airfoil. The forward scattered light from particles passing through the volume formed by the intersection of the four beams was optically collected and transmitted to photomultiplier tubes. The probe volume was approximately 0.3 mm in diameter with a length of approximately 3 mm in the spanwise direction. Bragg cells were used to enable the system to detect velocity direction by causing the fringes within the stationary measuring volume to move downstream at the Bragg frequency of 40 MHz. Vertical and chordwise movement of the probe volume during surveys was accomplished by remotely positioning the optical bench that supported the laser and optics.

A two-channel, synchronized counter system developed at Ames Research Center measured the velocity of particles passing through the probe volume. Pulse stretching, velocity consistency checks on the basis of particles crossing 5 and 8 fringes, and signal-amplitude limiting were employed. A diagram of the system is shown in Fig. 3b.

Two data acquisition modes were used during these tests. For the steady flow case (see Mode I, Fig. 3b), doppler frequencies were processed by the counters and passed into a dual-channel signal analyzer which retained the data in memory. Subsequent to the completion of data acquisition, a computer with access to this memory was used to determine statistically the mean velocities and their variances. The doppler frequencies processed by the counters for the unsteady flow case (see Mode II, Fig. 3b) were conditioned by an interface and recorded with an analog tape recorder to retain real-time information.

The flow was seeded by introducing 0.4-μm-diam polystyrene spheres into the settling chamber of the facility upstream of the model. This was necessary because of a lack of naturally occurring particles in the air supply system. An analysis of the response of the seed spheres to a normal shock wave indicated that a 99% velocity adjustment would occur in a distance of about 1 mm (Ref. 9). A counting rate of a few thousand per second was obtained, which was sufficient for this investigation.

The optical arrangement, incident beam wavelength, and the resulting doppler frequency uniquely determine the velocity of a particle passing through the probe volume in the direction normal to the fringes. Expressions for determining the mean velocity, shear stress, and turbulent kinetic energy, taken from Ref. 10, were evaluated from the frequency data stored in memory.

Computations and Turbulence Models

The flowfield was numerically simulated with a computer program that solves the Reynolds averaged form of the Navier-Stokes equations. The governing equations and solution procedure are discussed in Ref. 11. The program used an explicit finite-difference method that employs operator splitting and a recently developed rapid solver technique.[12] The flow around the complete airfoil was computed and the wind-tunnel walls incorporated in the outer boundary conditions.[8]

The Reynolds stresses were related to the mean flow by introducing the concept of a scalar eddy viscosity

$$\tau_t = \rho\epsilon\left(\frac{\partial u}{\partial y} + \frac{\partial v}{\partial x}\right) \tag{1}$$

The turbulence model employed was introduced in Ref. 8. Expressions used for the eddy viscosity coefficient in the regions of the boundary layer and wake indicated in Fig. 4 are listed below.

Inner Region (I)

$$\epsilon = \ell^2\left[\left(\frac{\partial u}{\partial y}\right)^2 + \left(\frac{\partial v}{\partial x}\right)^2\right]^{1/2} \tag{2}$$

$$\ell = 0.41y[1 - \exp(-y/A)] \tag{3}$$

where the Van Driest damping length is

$$A = 26\frac{\mu_w}{\rho_w}\left(\frac{\rho_w}{|\tau_w|}\right)^{1/2} \tag{4}$$

Outer Region (II) of Boundary Layer and Wake

$$\epsilon = \ell^2\left[\left(\frac{\partial u}{\partial y}\right)^2 + \left(\frac{\partial v}{\partial x}\right)^2\right]^{1/2} \tag{5}$$

where an Escudier formulation was used for the length scale,[13]

$$\ell = 0.09(y_\delta - y_{DS}) \tag{6}$$

In region II over the separated bubble (regions III and IV), ℓ, is frozen at the value evaluated at the first computational chordwise station upstream of separation.

Separation Bubble Wall Region (III)

$$\rho\epsilon = (\rho\epsilon)_{DS}\left(\frac{y - y_w}{y_{DS} - y_w}\right) \tag{7}$$

Separation Bubble Wake Region (IV)

$$\rho\epsilon = (\rho\epsilon)_{DS} \tag{8}$$

Results and Discussion

Steady Flow with Shock-Induced Separation

Experimental Observations

A shadowgraph of the flowfield taken through the test section windows during a test at $M_\infty = 0.79$ and $Re_c = 11 \times 10^6$ is shown in Fig. 5. At these test conditions shock-induced separation occurs near the foot of the shock wave and extends downstream beyond the trailing edge. A highly turbulent flow exists downstream of the shock wave and Mach waves appear to emanate from the interface between the turbulent shear

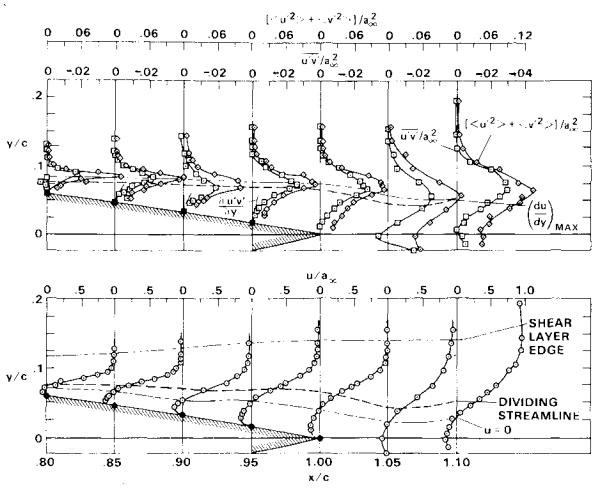

Fig. 6 Mean velocity, turbulent shear stress, and kinetic energy profiles in the shear layer downstream of separation, $M_\infty = 0.79$ and $Re_c = 11 \times 10^6$.

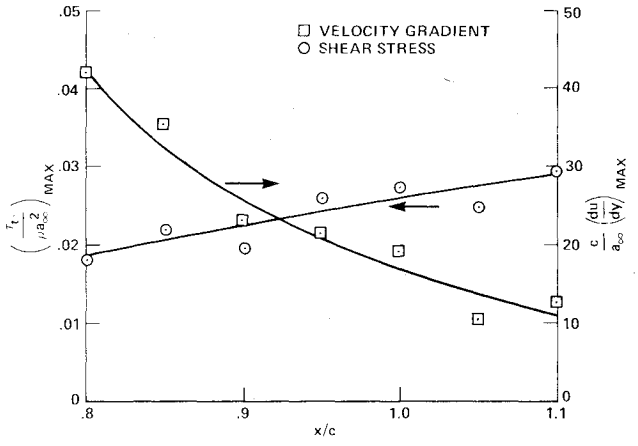

Fig. 7 Variation of maximum shear stress and velocity gradient in shear layer downstream of separation, $M_\infty = 0.79$ and $Re_c = 11 \times 10^6$.

layer and the outer flow. Superimposed on the shadowgraph are mean axial velocity profile data obtained with the laser velocimeter.

The mean streamwise velocity, turbulent shear stress, and turbulent kinetic energy for the viscous region of the flow downstream of the separation point are shown in Fig. 6. The airfoil surface has been sketched in the figure and the solid symbols indicate the respective wall values. The wall shear values were published previously.[14] Lines are sketched in the lower half of Fig. 6 through a locus of points representing the locations of the zero velocity point, the dividing streamline, and the shear-layer edge. In the upper half of the figures are lines representing the dividing streamline and the location of the maximum axial velocity gradient in the normal direction. The slopes of the shear profiles at the wall, obtained by evaluating the streamwise momentum equation, are shown in Fig. 6 for a more complete picture of the profiles and for assistance in assessing the accuracy and interpretation of the near-wall data. The shear stress data at $x/c = 0.8$ below the location of their maximum are anomalous in that they change sign. Possibly they are in error; however, since a postrun examination of the data revealed no obvious sources of error, they have been included.

An examination of the profile shapes in Fig. 6 reveals that the maximum values of the shear stress and turbulent kinetic energy are located somewhat above the dividing streamline and generally coincide with the location of the maximum velocity gradient. The magnitude of the maximum velocity gradient decreases with distance from the separation point whereas the magnitude of the maximum shear stress increases (Fig. 7).

The profile shapes and their behavior in the streamwise direction compare with similar data taken downstream of separation in a transonic flow over a bump on a wind-tunnel wall[15] as well as downstream of rearward facing steps ahead of reattachment.[16-18] Bradshaw[19] classified the latter flows, in which the step height was larger than the upstream boundary-layer thickness, as flows undergoing an overwhelming perturbation and postulated that the development of the free-shear-layer was not influenced significantly by its initial conditions such as upstream boundary-layer thickness or shape parameter, and that production of turbulence continued in proportion to the growth of the large-scale structure until reattachment occurred. The present shock-separated flow appears to behave similarly; the extent of the shock-induced separation and the airfoil surface pressures were unaffected by changes in test Reynolds number between 7×10^6 and 17×10^6 (Ref. 7). The shock-wave induced separation produced significant large-scale turbulence, and production continued beyond the trailing edge into the near wake until its eventual dissipation in the far wake. The recirculation region was supplied continually by the higher turbulent portion of the shear layer. Because of the limited streamwise extent of the test section windows, it was impossible to identify optically the entire near-wake region. An oil-flow photograph (Fig. 8) indicates the approximate size and location of the near-wake region.§ The pattern of oil streaks was allowed to develop on a thin splitter plate located near the midspan of the airfoil in a plane normal to the spanline. In the near-wake region the oil streaks begin to flow in the downstream direction indicating closure at $x/c \approx 1.3$. The necking down of the zero velocity and the dividing streamlines in the near wake at $x/c = 1.05$ observed in the velocity profile data is also apparent from a close examination of a number of such photographs.

The values of surface pressure and skin friction have been reported previously.[7,14] They are shown in Fig. 9 for completeness and because they are needed to assess the computations discussed subsequently. The data show a small pressure recovery aft of the shock-induced separation point. The magnitude of the pressure coefficient downstream of separation is slightly lower than C_p^* and the flow may be slightly supersonic. This interpretation is consistent with the shadowgraph observation (Fig. 5) which revealed an oblique shock near the separation point. Additionally, the Mach number at the edge of the shear layer, evaluated by solving the energy equation using the measured velocities, shock angles, and total temperature was found to be slightly supersonic.

The data from Fig. 6 can be used to guide turbulence model development for use in computer codes that attempt to simulate complicated viscous flow numerically. Thus far, simulations using the Reynolds averaged Navier-Stokes equations have utilized a scalar eddy diffusivity formed from a product of a modeled length scale and velocity.[4,5,8,20,21] The shear stress and velocity profile data were used to deduce the eddy diffusivity, and the results are shown in Fig. 10 as a function of the position within the shear layer. Since derivatives of the velocity are needed to evaluate the eddy diffusivity, no values are shown for the first measuring station away from the surface where the derivative was undetermined. Likewise no values are shown at the edge of the shear layer where accurate derivative evaluation was not possible. A general observation is that the eddy diffusivity tends to increase with distance downstream from the separation point and its maximum value tends to diffuse outward through the shear layer, particularly beyond the trailing edge. At streamwise locations where the maximum value is readily distinguished it occurs at the point where the normal velocity gradient is maximum.

§This photograph, supplied by John McDevitt from Ames Research Center, was taken during a separate series of tests.

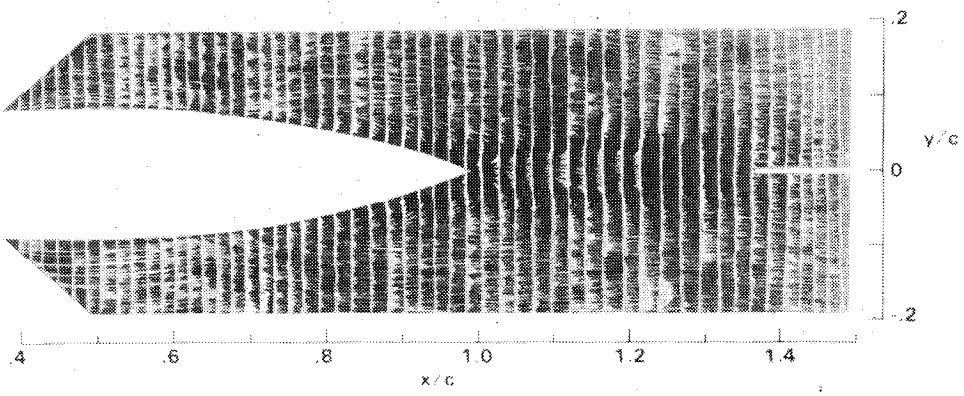

Fig. 8 Oil flow photograph showing qualitative flow features for steady shock-induced separation.

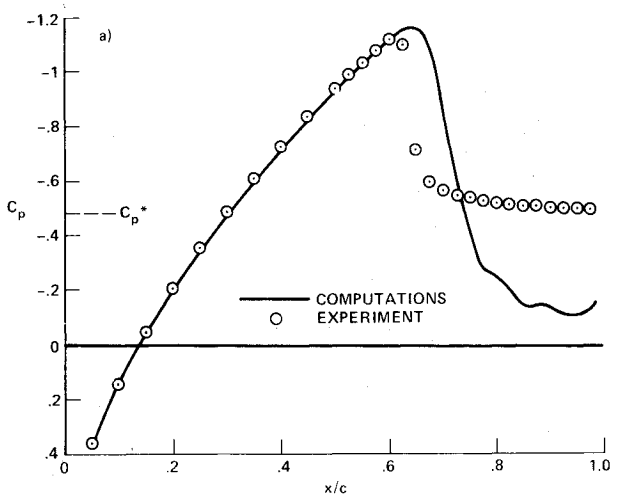

a) Pressures

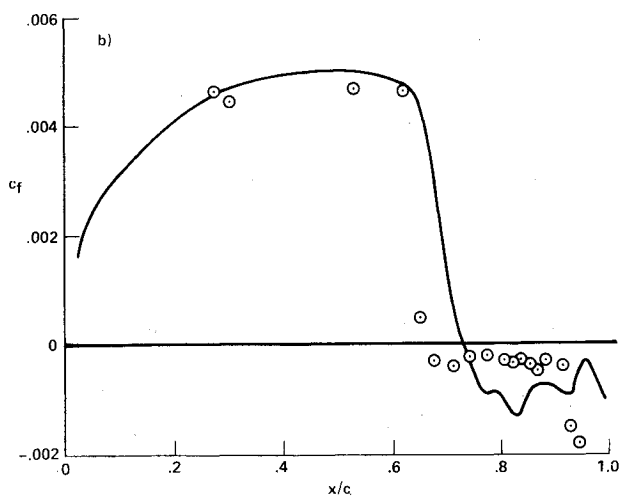

b) Skin friction

Fig. 9 Experimental and computed pressures and skin friction on the airfoil surface, $M_\infty = 0.79$ and $Re_c = 11 \times 10^6$.

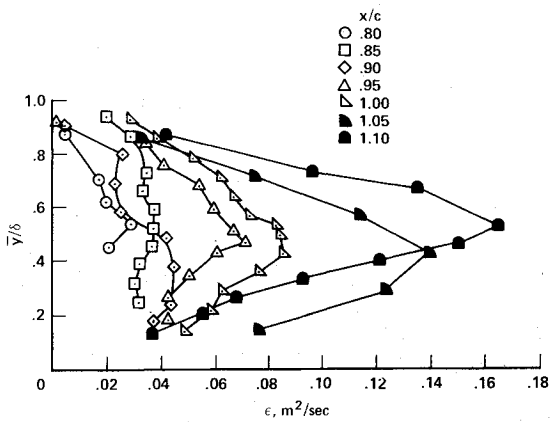

Fig. 10 Eddy diffusivity profiles in the shear layer downstream of separation, $M_\infty = 0.79$ and $Re_c = 11 \times 10^6$.

The algebraic mixing length deduced from the data was obtained using Eq. (5) without $(\partial v/\partial x)$ (Fig. 11a). The length scale over the airfoil surface tends to correlate when normalized by the shear-layer thickness. The magnitude for most of the shear layer is lower than the Escudier value employed for attached boundary-layer flows, however. Beyond the trailing edge the normalized length scale tends to increase and is in closer agreement with the Escudier value. Although every attempt was made to obtain data as close to the airfoil surface as possible, the paucity of data makes it difficult to interpret the behavior of the length scale in the near-wall region.

Some improvement in modeling for a class of shock boundary-layer interaction flows was obtained by employing a modified Glushko model[20] which uses the turbulent kinetic energy and an algebraic length scale based on the mean flow to formulate the eddy viscosity, i.e., $L \approx \epsilon/\sqrt{k}$ (Ref. 21). (To form the total kinetic energy from the measurements of $\langle u'^2 \rangle + \langle v'^2 \rangle$ the relationship $\langle u'^2 \rangle : \langle w'^2 \rangle : \langle v'^2 \rangle = 4:3:2$ was assumed.) This length scale (Fig. 11b) correlates with boundary-layer thickness over the airfoil and is smaller than the algebraic scale employed by Glushko for boundary layers (the line labeled *ao*). The line labeled *bo* represents the modified length scale employed[21] to achieve thicker separated bubbles in other shock boundary-layer interaction flows and it agrees more closely with the present data. Downstream of the trailing edge this length scale also increases.

The appropriateness of a scalar eddy diffusivity cannot be established solely on the basis of the present data. However, in light of the similarities in the data above the zero velocity line to those observed in free-shear layers successfully modeled through such an approach, the concept seems credible. The maximum shear occurs at the location of the maximum normal velocity gradient. A length scale model for the eddy diffusivity may even be appropriate, but some means would have to be established for varying it to account for the sudden growth in the near wake.

Comparison with Computations

A comparison of numerical computations with surface pressure and skin-friction data is given in Fig. 9. The governing equations and the model of turbulence were discussed previously. Ahead of the shock-wave location the surface pressures are well predicted, but the pressure recovery is too large over the rear portion of the airfoil where separation occurs. The skin-friction prediction shows reasonable agreement with the experiment, except near the location of separation and in the variation through the separated region. The code fails to give the appropriate pressure in the separated region because the predicted shock wave is nearly normal whereas in the experiment it is oblique in the region near the wall where separation is occurring.

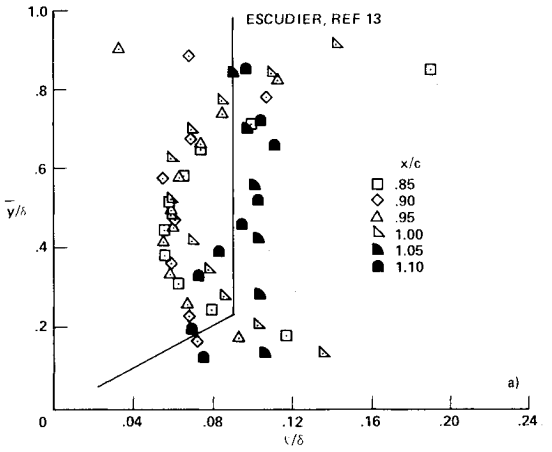

a) Prandtl mixing length

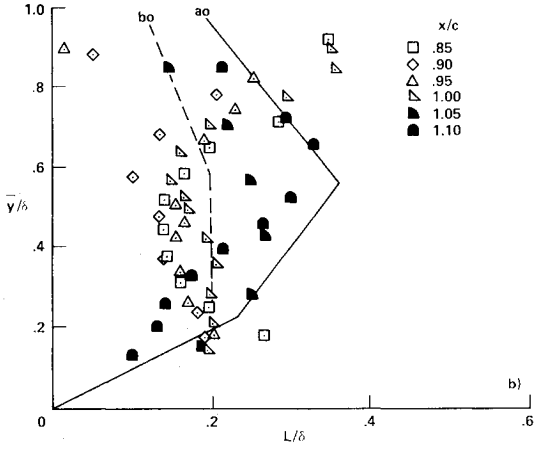

b) Glushko length scale

Fig. 11 Length scales measured in the shear layer downstream of separation, $M_\infty = 0.79$ and $Re_c = 11 \times 10^6$.

Whether this result is due to failure of the turbulence model or to failure of the code to predict a weak shock-wave solution in the inviscid regions of the flow cannot be answered readily because of the complex interaction between the viscous and inviscid regions of the flow. However, it is possible to assess the appropriateness of the turbulence model in light of the experimental data introduced previously.

A comparison of the computation with the velocity and eddy diffusivity deduced from the experiment at two chordwise locations on the airfoil is presented in Fig. 12. (Comparisons at other locations show similar results.) The predicted separation height is smaller than that determined experimentally. The maximum eddy diffusivities compare, but their relative position in the boundary layer differ because the computed shear layer is too thin. The main deficiency of the computation is that of underpredicting both the separation region and outer shear layer thickness relative to the experiment. Considering the complexity of the flow under study, the predicted results, while deficient in some aspects, do reproduce many of the correct features of the flow and hence the numerical simulations are encouraging.

Unsteady Flow with Shock-Induced Separation

Experimental Observations

The flow over the airfoil at zero incidence was found to be unsteady for a narrow range of Mach numbers. This observation was first reported in Ref. 7 and introduced previously in Fig. 2. A portion of the experimental surface pressure time histories taken during a Mach number sweep through the unsteady flow region for two positions on the

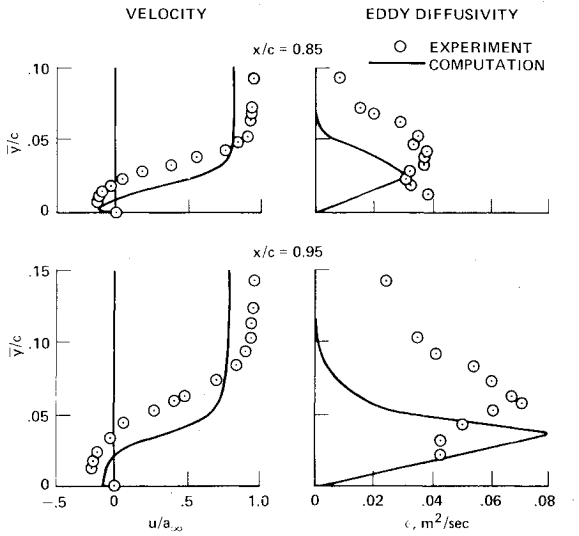

Fig. 12 Comparison of experimental and computed velocity and eddy diffusivity profiles $M_\infty = 0.79$ and $Re_c = 11 \times 10^6$.

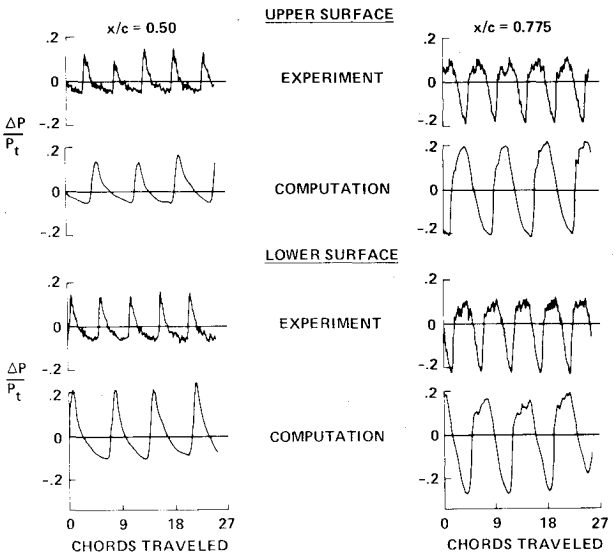

Fig. 13 Surface pressure time histories on the airfoil with unsteady flow, $M_\infty = 0.76$ and $Re_c = 11 \times 10^6$.

airfoil are shown in Fig. 13. These pressures, expressed as an incremental difference from the mean, are shown as a function of a dimensionless time required for the flow to travel from the leading to the trailing edge, tu_∞/c. Examination of these data shows that the unsteady pressures are periodic and that the pressures on the upper and lower surface are 180 deg out of phase. The frequency of oscillation was found to be independent of position and its value was 188 Hz. The calculations shown on the figure will be discussed later.

A high-speed shadowgraph movie of the flowfield was taken during a test at $M_\infty = 0.76$. A pulse triggered from the initial rise in the output of the periodic pressure signal on the airfoil at $x/c = 0.5$ was recorded on the film and used to synchronize these photographs with the pressure signal. Film speeds as high as 10,000 frames/s were used. At the time of the initial rise in the pressure, the remnants of a shock wave passing upstream near the midchord of the airfoil were visible. Photographs taken from subsequent frames of the films are shown in Fig. 14a. A series of weak shock waves form near the trailing edge where they build in strength and coalesce into a single wave that moves toward the midchord. As the shock approaches the midchord it weakens appreciably and the cycle repeats itself periodically. A similar situation occurs on the lower surface 180 deg out of phase. A vortex is

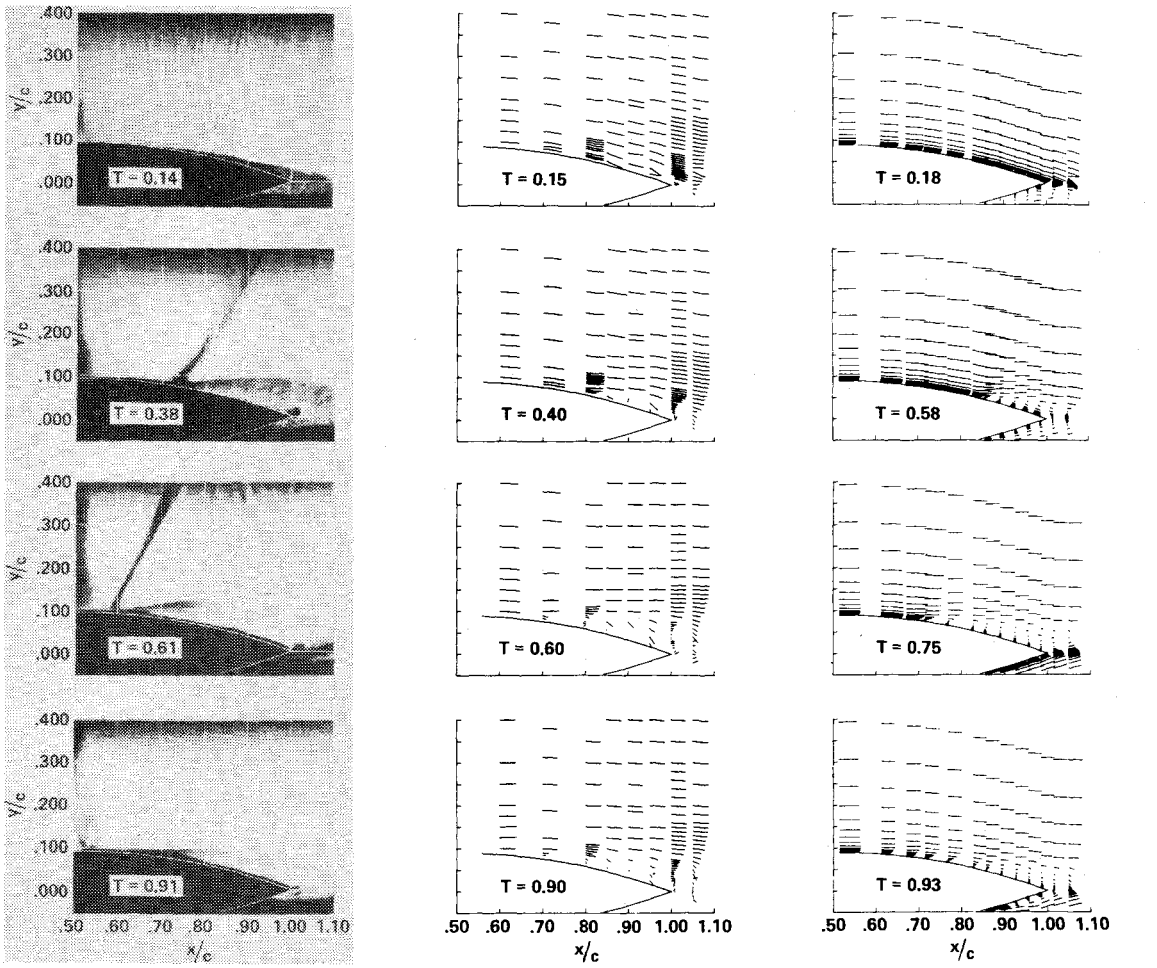

a) Shadowgraphs b) Velocity field from the experiment c) Velocity field from the computation

Fig. 14 Flowfield over the airfoil with unsteady flow, $M_\infty = 0.76$ and $Re_c = 11 \times 10^6$.

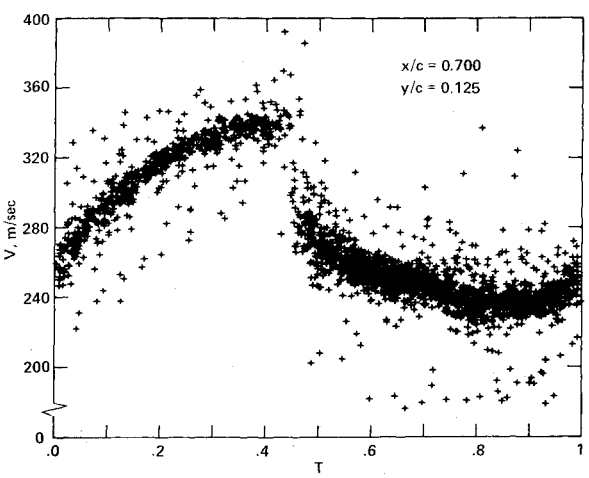

Fig. 15 Time-history of velocity from conditionally sampled data for one cycle of flow oscillation, $M_\infty = 0.76$ and $Re_c = 11 \times 10^6$; $x/c = 0.7$ and $y/c = 0.125$.

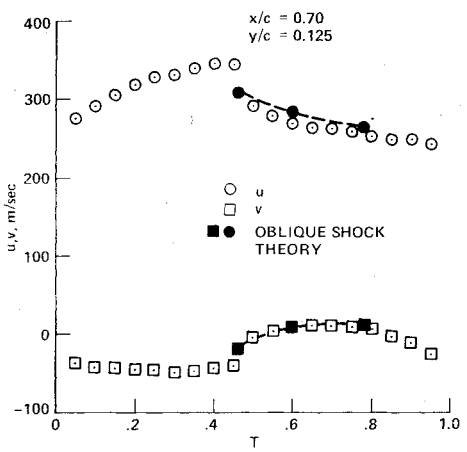

Fig. 16 Time history of mean velocity components from conditionally sampled data for one cycle of flow oscillation, $M_\infty = 0.76$ and $Re_c = 11 \times 10^6$; $x/c = 0.7$, and $y/c = 0.125$.

seen to form near the trailing edge and sheds alternately upward and downward, depending on the direction of the asymmetry of the periodic flow. The remaining portions of the figure will be discussed subsequently.

The laser velocimeter was used to determine the velocity field during the flow oscillations. Instantaneous u and v velocities were recorded on an analog tape recorder along with the signal from a pressure transducer located at midchord. The data were digitized and the velocities conditionally sampled relative to an initial time triggered by the onset of the steep rise in each successive pressure signal. An example of the conditionally sampled data for a single point in the flowfield is shown in Fig. 15. The magnitude of the total velocities is shown as a function of the dimensionless fraction of time T for one cycle of oscillation. Over 2000 synchronous data samples were used to construct this plot. The velocity increases with time initially and then shows a marked decrease as the shock wave passes upstream.

Velocity data at 125 points in the flowfield were acquired in the manner just described. To keep data management tolerable, a mean value of velocity was determined by

averaging the data over discrete dimensionless time intervals of 0.05. The resultant time history of the mean velocity components of the data shown in Fig. 15 are given in Fig. 16 to illustrate two points. First, the data can be used to determine the direction of the flow, $\bar{\theta} = \tan^{-1} v/u$. A cursory examination of the vertical velocity component shows that for $T < 0.4$ the flow is in a direction almost parallel to the airfoil surface. As the shock passes ($T > 0.45$) $\bar{\theta}$ approaches zero and goes slightly positive; the resultant flow angle is nearly parallel to the airfoil chord and subsequently returns to its initial value. Second, the correspondence between the solid and open symbols shows that the particles are able to adjust rapidly to the instantaneous change in velocity across the shock wave. The solid symbols represent velocities calculated from simple shock theory using the measured velocities ahead of the shock wave and the shock wave angles measured from the shadowgraphs. The slight departure from the u velocity data with distance downstream of the shock wave is associated with the compression process occurring between the shock wave and measuring point as the shock moves upstream (rather than with particle lag).

The complete velocity field over the airfoil obtained with the laser velocimeter is shown in Fig. 14b. Data are shown which correspond as closely as possible to the times for the shadowgraphs. (Space limitations preclude showing data at more time intervals, but a movie showing data for 20 equally spaced intervals was made to aid data interpretation.) The lines representing the velocity vectors are in arbitrary units. The origins of the vectors can be determined by inspection of the data for the first time interval, where all of the flow is in the downstream direction. The small group of vectors near the trailing edge at $x/c = 1.007$ overlap those at $x/c = 1.0$ farther away from the surface. Examination of the velocity field data and the shadowgraphs for all 20 time intervals reveals a rather complete picture of the flowfield. As the shock wave begins to form near the rear of the airfoil, it strengthens and moves upstream. Separation occurs at the foot of the shock with subsequent reattachment on the airfoil surface. Downstream at the trailing edge a small vortex is formed and circulation occurs from the airfoil surface with attached flow, around the trailing edge, to the surface with shock separated flow.

Comparisons with Computations

Computations using the Navier-Stokes code and the turbulence model discussed earlier have been made in each of the flow domains shown in Fig. 2. As noted in Ref. 8, these computations reproduced flow features observed experimentally. A more thorough evaluation for the unsteady case is made herein.

A comparison with the experimental surface pressure time histories is shown in Fig. 13. The wave forms of the fluctuating pressures, obtained by computing four cycles of oscillation, compare rather well with the experimental forms. The oscillations on the upper and lower surfaces are 180 deg out of phase as observed experimentally. However the normalized frequency of oscillation (fc/u_∞) is about 20% lower. On the upper surface at the midchord the magnitudes of the peak fluctuations on either side of the mean compare favorably with the experiment. At $x/c = 0.775$ the magnitude of the negative peak fluctuations compare, but the positive magnitudes are about twice that of the experiment. This is consistent with the fact that the computation tends to overpredict the pressure recovery downstream of the shock.

Computed velocity fields for selected fractions of the time within a cycle of oscillation are shown in Fig. 14c. These times differ from those chosen for the experiment for reasons that will become apparent later. As time increases, a shock begins to form on the upper surface as evidenced by the change in magnitude of the vectors and also their direction. The shock continues to move forward and separation occurs with reattachment near the trailing edge. Subsequently, the shock

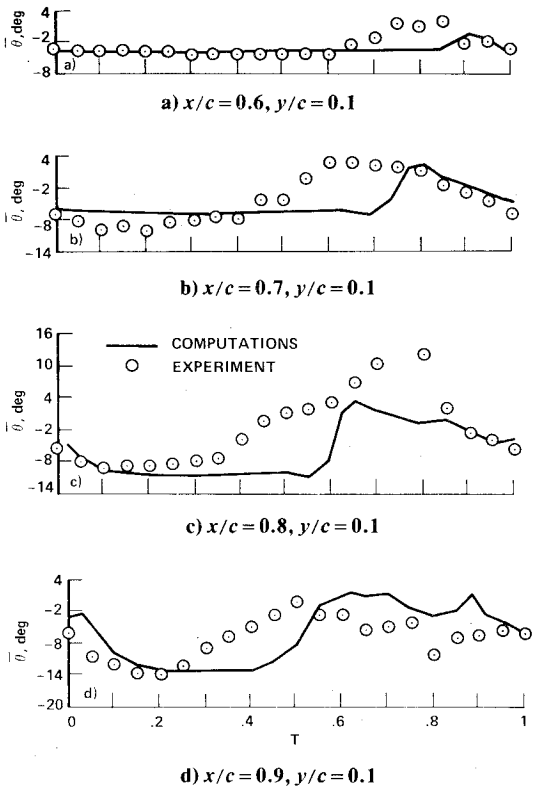

a) $x/c = 0.6, y/c = 0.1$

b) $x/c = 0.7, y/c = 0.1$

c) $x/c = 0.8, y/c = 0.1$

d) $x/c = 0.9, y/c = 0.1$

Fig. 17 Mean flow direction for one cycle of flow oscillation, $M_\infty = 0.76$ and $Re_c = 11 \times 10^6$.

continues forward and large-scale vortical flow or shedding appears just beyond the trailing edge.

The predicted shock formation and its subsequent movement toward the leading edge took a longer portion of the cycle time than in the experiment. Therefore the comparisons of the velocity fields in Fig. 14 were made at somewhat different times so that similar flow features could be compared. The flow angle histories at several chordwise stations at $y/c = 0.1$ are compared in Fig. 17 to illustrate this difference. In each example the initial increase in angle can be associated with the shock-wave movement across the measuring point. Although the time of shock arrival is longer for the computation, the resulting change in flow angle is more abrupt.

The computation was studied in an attempt to explain the onset and maintenance of the unsteady flow. Sequential development of the flowfield showed that the probable process that initiated the unsteady flow depended on two conditions. The first was a slight asymmetry in the location of the separation points on the upper and lower surfaces caused by a code asymmetry. Freestream flow angle or model construction asymmetry may have introduced similar differences experimentally. The second was rapid development of a single separation zone on one side of the airfoil where the separated region behind the shock and the separated region at the trailing edge joined. The resulting asymmetry in the wake tends to extract mass from the trailing-edge separated region on the other side of the airfoil, momentarily preventing the development of a single separation on that side. Meanwhile the outer inviscid flow adjusts to the displacement effects as if the airfoil had been given camber, and the flow slows with a subsequent weakening of the shock wave until the separation collapses. Thus, the sequence of oscillation is set; the flow on the opposite side speeds up and the stronger shock separates the flow causing the process to continue.

If this physical description is correct, the period of oscillation would then depend on the time it takes for the entire flow to adjust to the displacement effects caused by the

thickening shear layers. Two important findings support this. First, the experimental reduced frequency, $\pi fc/u_\infty$, compares with that observed by Finke[22] in another investigation using circular arc airfoils of different chord dimensions, where the Reynolds number was much lower. The second is that the reduced frequency determined from the present computation compared exactly with a different computation in which the airfoil chord dimension was halved.

Conclusions

A study of the transonic flow over a circular arc airfoil was undertaken to provide guidance for turbulence modeling of shock-induced separated flows and to verify numerical computer codes that are being developed to simulate such flows. Depending on the freestream Mach number, the flowfield developed was either steady with shock-wave-induced separation extending from the foot of the shock wave to beyond the trailing edge or unsteady with a periodic motion also undergoing shock-induced separation. Mean velocity and turbulence measurements for the steady flow case were successfully made with a laser velocimeter. Mean-flow velocities were also obtained in the unsteady periodic flow with the same instrument by a conditional sampling technique using a pressure signal measured at the airfoil midchord. Comparisons with numerical simulations using a computer code that solved the time-dependent Reynolds' averaged compressible Navier-Stokes equations were made for both flow conditions.

For the steady flow case, a thick shear layer formed downstream of the shock-induced separation point. Within the shear layer the maximum turbulent kinetic energy and shear stress occurred at a location corresponding to that where the maximum normal velocity gradient occurred, thus supporting the appropriateness of a scalar eddy viscosity concept in the outer portions of the shear layer. Comparing the measurements with computations employing a mixing length model to describe the eddy viscosity showed that the shear-layer thickness was underpredicted and that the resulting influence on the outer flow gave a rather poor prediction of the actual pressure recovery on the airfoil.

In the unsteady flow case a shock wave formed on one surface near the trailing edge. As its strength increased, the flow separated just behind the shock wave and reattached on the airfoil. On the opposite surface a similar sequence took place, but 180 deg out of phase. Computations of the flow predicted most of the essential features observed experimentally, but the reduced frequency was lower by about 20%. The details of the computation were used to explain a possible sequence of events leading to the unsteady motion.

Acknowledgments

The authors wish to gratefully acknowledge the contributions of E. Pegot, D. Harrison, G. Grant, G. Kojima, and R. Hedlund.

References

[1]Murman, E. M. and Cole, J. D., "Calculation of Plane Steady Transonic Flows," *AIAA Journal*, Vol. 9, Jan. 1971, pp. 114-121.

[2]Bauer, F., Garabedian, P. R., and Korn, D., "A Theory of Supercritical Wing Sections, with Computer Programs and Examples," *Lecture Notes in Economics and Mathematical Systems*, Vol. 66, Springer-Verlag, C., 1972.

[3]Bailey, F. R. and Ballhaus, W. F., "Comparisons of Computed and Experimental Pressures for Transonic Flows about Isolated Wings and Wing-Fuselage Configurations," NASA SP-347, Vol. II, 1975, pp. 1213-1232.

[4]Deiwert, G. S., "Computation of Separated Transonic Turbulent Flows," *AIAA Journal*, Vol. 4, June 1976, pp. 735-740.

[5]Marvin, J. G., "Experiments Planned Specifically for Developing Turbulence Models in Computations of Flow Fields Around Aerodynamic Shapes," *AGARD Conference Proceedings No. 210 on Numerical Methods and Wind Tunnel Testing*, Paper No. 14, Von Karman Institute for Fluid Dynamics, Rhode-St-Genese, Belgium, June 23-24, 1976.

[6]Marvin, J. G, "Turbulence Modeling for Compressible Flows," NASA TM X-73,188, Jan. 1977.

[7]McDevitt, J. B., Levy, L. L. Jr., and Deiwert, G. S., "Transonic Flow About a Thick Circular-Arc Airfoil," *AIAA Journal*, Vol. 14, May 1976, pp. 606-613.

[8]Levy, L. L., Jr., "Experimental and Computational Steady and Unsteady Transonic Flows About a Thick Airfoil," *AIAA Journal*, Vol. 16, June 1978, pp. 564-572.

[9]Maxwell, B. R. and Seasholtz, R. G., "Velocity Lag of Solid Particles in Oscillating Gases and in Gases Passing Through Normal Shock Waves," NASA TN D-7490, March 1974.

[10]Yanta, W. J., "Turbulence Measurements with a Laser Doppler Velocimeter," Ph.D. Thesis, The Catholic University of America, Washington, D.C., 1973.

[11]Baldwin, B. S., MacCormack, R. W., and Deiwert, G. S., "Numerical Techniques for the Solution of the Compressible Navier-Stokes Equations and Implementation of Turbulence Models," AGARD LSP-73, 1975.

[12]MacCormack, R. W., "An Efficient Numerical Method for Solving the Time-Dependent Compressible Navier-Stokes Equations at High Reynolds Number," NASA TM X-73,129, July 1976.

[13]Escudier, M. P., "The Distribution of the Mixing Length in Turbulent Flow Near Walls," Imperial College, London, Rept. TWF/TN/1, 1965.

[14]Rubesin, M. W., Okuno, A. F., Levy, L. L., Jr., McDevitt, J. B., and Seegmiller, H. L., "An Experimental and Computational Investigation of the Flow Field About a Transonic Airfoil in Supercritical Flow With Turbulent Boundary-Layer Separation," *10th Congress of the International Council of the Aeronautical Sciences*, Ottawa, Canada, Oct. 4-8, 1976; also NASA TM X-62,465, July 1976.

[15]Alstatt, M. C., "An Experimental and Analytical Investigation of a Transonic Shock-Wave-Boundary-Layer Interaction," Arnold Engineering Development Center, Tenn., AEDC TR 77-47, May 1977.

[16]Arie, M. and Rouse, H., "Experiments on Two-Dimensional Flow Over a Normal Wall," *Journal of Fluid Mechanics*, Vol. 1, July 1956, p. 129.

[17]Tani, I., Iuchi, M., and Komodu, H., "Experimental Investigation of Flow Separation Associated with a Step or a Groove," Aeronautical Research Institute, University of Tokyo, Rept. No. 364, April 1961.

[18]Le Balleur, J.-C., and Mírande, J., "Experimental and Theoretical Study of Two-Dimensional, Turbulent, Incompressible Reattachment," *AGARD Meeting on Separated Flow*, Göttingen, May 27-30, 1975, pp. 17-1-17-13 (NASA Technical Translation).

[19]Bradshaw, P. and Wong, F.Y.F., "The Reattachment and Relaxation of a Turbulent Shear Layer," *Journal of Fluid Mechanics*, Vol. 52, Pt. 1, March 14, 1972, pp. 113-135.

[20]Rubesin, M. W., "A One Equation Model of Turbulence for Use With the Compressible Navier-Stokes Equations," NASA TM X-73,128, April 1976.

[21]Coakley, T. J., Viegas, J. R., and Horstman, C. C., "Evaluation of Turbulence Models for Three Primary Types of Shock Separated Boundary Layers," Paper 77-692, Albuquerque, New Mex., June 1977.

[22]Finke, K., "Unsteady Shock-Wave Boundary-Layer Interaction on Profiles in Transonic Flow," AGARD-CPP-168, Paper 28, 1975.